ResearchGate

See discussions, stats, and author profiles for this publication at: https://www.researchgate.net/publication/265909201

A significant role of Arg41 residue in the enzymatic reaction of haloacid dehalogenase L-DEX YL studied by QM/MM method

ARTICLE *in* JOURNAL OF MOLECULAR CATALYSIS B ENZYMATIC · DECEMBER 2014

Impact Factor: 2.13 · DOI: 10.1016/j.molcatb.2014.09.006

CITATION
1

READS
49

3 AUTHORS, INCLUDING:

Shigenori Tanaka
Kobe University
176 PUBLICATIONS **2,715** CITATIONS

SEE PROFILE

Available from: Shigenori Tanaka
Retrieved on: 15 January 2016

Journal of Molecular Catalysis B: Enzymatic 110 (2014) 23–31

Contents lists available at ScienceDirect

Journal of Molecular Catalysis B: Enzymatic

journal homepage: www.elsevier.com/locate/molcatb

A significant role of Arg41 residue in the enzymatic reaction of haloacid dehalogenase L-DEX YL studied by QM/MM method

Hirotaka Kondo[a,*], Takashi Nakamura[b], Shigenori Tanaka[c,*]

[a] Graduate School of Human Development and Environment, Kobe University, 3-11 Tsurukabuto, Nada, Kobe 657-8501, Japan
[b] Nagahama Institute of Bio-Science and Technology, 1266 Tamura, Nagahama, Shiga 526-0829, Japan
[c] Graduate School of System Informatics, Kobe University, 1-1 Rokkodai, Nada, Kobe 657-8501, Japan

ARTICLE INFO

Article history:
Received 7 April 2014
Received in revised form 23 August 2014
Accepted 12 September 2014
Available online 22 September 2014

Keywords:
Enzymatic reaction
2-Haloacid dehalogenase
L-2-Chloropropionic acid
ONIOM method
Transition state

ABSTRACT

L-2-Haloacid dehalogenase (L-DEX) is one of a family of enzymes that decompose a variety of environmental pollutants such as L-2-chloropropionate (L-2-CPA). This enzyme specifically produces a D-2-hydroxy acid from a L-2-haloacid, and, to date, some residues have been suggested as important in this enzymatic reaction. Here, quantum-mechanical (QM)/molecular-mechanical (MM) calculations for the L-DEX from *Pseudomonas* sp. YL (L-DEX YL) 2-CPA complex were performed to elucidate the structure of transition state and the energy profile in this enzymatic reaction. QM/MM simulations using the ONIOM (PM3:Amber) method revealed that the activation energy of dehalogenation reaction was around 9.0 kcal/mol and that one of the most important residues in the ester intermediate formation step was Arg41, which was found to decrease the activation energy by about 40 kcal/mol compared to the case of its absence. On the other hand, this stabilization effect by Arg41 was significantly counterbalanced by the presence of Asn177. Simulations of enzymes mutated at Arg41 indicated that mutants possessing a positive charge near the Arg41 position would allow the dehalogenation reaction as well. Specifically, it was suggested by our simulations that homolysine (homK) mutant of Arg41, which contains one more methylene group in the side chain compared to lysine, could be active as well as the wild-type enzyme. The distance from the chloride ion to the position of the positive charge of the acceptor seems to dictate the activation energy.

© 2014 Elsevier B.V. All rights reserved.

1. Introduction

Many organohalogen compounds are known to be produced biologically or by natural abiogenic processes [1]. Produced in large quantities by the chemical industry due to their usefulness as solvents, pharmaceuticals, and agrochemicals, these chemicals also cause serious environmental pollution and health problems. Dehalogenases detoxify various halogen compounds, catalyzing the removal of a halogen atom from their substrates, and are useful in environmental technology to decontaminate environments polluted with harmful organohalogen compounds.

2-Haloacid dehalogenases have been extensively studied and reviewed [2,3]. One dehalogenase, L-2-haloacid dehalogenase (L-DEX), catalyzes the hydrolytic dehalogenation of L-2-haloalkanoic acids to produce the corresponding D-2-hydroxyalkanoic acids with the release of halide ions. A representative enzyme of the haloacid dehalogenase superfamily, L-DEX, has been isolated and purified from several microbial strains [4]. L-DEX YL was isolated from *Pseudomonas* sp. strain YL cell culture in a medium containing 2-chloropropionate (2-CPA) as the sole carbon source [5]. The reaction mechanisms of L-DEX YL have been analyzed by site-directed mutagenesis [6], X-ray crystallography [7–9], mass spectrometry [10–12], ^{18}O-incorporation experiments [13], and computer simulations by the molecular dynamics and fragment molecular orbital methods [14].

Site-directed mutagenesis experiments have revealed that those amino acid residues such as Asp10, Thr14, Arg41, Ser118, Lys151, Tyr157, Ser175, Asn177 and Asp180 are important for the catalytic function of L-DEX YL [6]. ^{18}O-incorporation experiments have revealed that Asp10 plays a pivotal role in a nucleophilic attack on a substrate α-carbon to form an ester intermediate, which is then hydrolyzed by water [13]. These studies suggest the reaction mechanism shown in Fig. 1. Mass spectrometry analysis has shown the involvement of Arg41 and Asp180 in the formation of an ester intermediate [12]. X-ray crystallographic analysis of L-DEX YL has provided further evidence for the formation of an

* Corresponding authors. Tel.: +81 078 803 6620; fax: +81 078 803 6621.
E-mail addresses: kondo@eniac.scitec.kobe-u.ac.jp (H. Kondo), t_nakamura@nagahama-i-bio.ac.jp (T. Nakamura), tanaka2@kobe-u.ac.jp (S. Tanaka).

http://dx.doi.org/10.1016/j.molcatb.2014.09.006
1381-1177/© 2014 Elsevier B.V. All rights reserved.

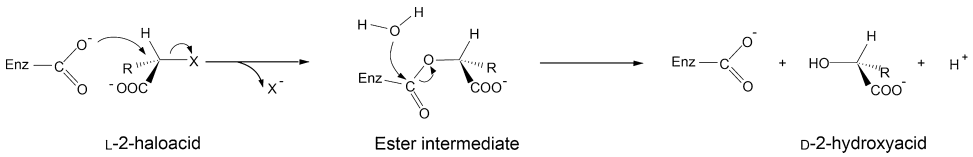

Fig. 1. The reaction mechanism of L-DEX YL. L-2-haloacid dehalogenases catalyze hydrolytic dehalogenation of L-2-haloalkanoic acids to produce corresponding D-2-hydroxyalkanoic acids with release of halide ion. X and R mean halogen and alkyl group including hydrogen, respectively.

ester intermediate and information on the functions of active-site amino acid residues [7,8].

Before attempting to improve those L-DEX YL functions such as catalytic efficiency and substrate specificity, it is important to clarify the transition state (TS) structure of the enzyme and elucidate its catalytic mechanism at the molecular level. Although the TS structures have already been determined in haloalkane dehalogenase [15,16] and fluoroacetate dehalogenase [17], that of L-DEX has not yet been determined and examined only through simulations based on the crystal structure [18], molecular dynamics and the fragment molecular orbital method [14]. In this study, we focused on the first step involving the Asp10 nucleophilic attack on the C2 atom of the substrate to produce an ester intermediate and halide ion. The TS structure in the formation of the ester intermediate of L-DEX YL and L-2-chloropropionate (L-2-CPA) was determined; the reaction mechanism of this step and the roles of amino acid residues in the active site were thus analyzed on the basis of quantum-mechanical/molecular-mechanical (QM/MM) calculations. In addition, site-directed mutagenesis simulations were employed to predict the effects of the mutation of a single, significant residue for the purpose of designing more reactive mutant enzymes.

2. Computational details

2.1. Preparation of the starting geometries

Using the method by Nakamura et al. [14], the initial enzyme structure was constructed from the atomic coordinates of L-DEX YL, obtained from Protein Data Bank (PDB entry: 1ZRM) [8]. The PDB structure with the mutation of S175A was then modified to the wild-type structure and the L-2-CPA was docked instead of L-2-chloro-*n*-butyrate, using Molecular Operating Environment (MOE) software [19], Alpha Site Finder [20], and ASEDock2005 (ver. 2006.07.31) [21]; the docking simulation and the energy minimization were performed with Amber8 [22].

Since the protonation state is significant for the enzymatic reaction, we carefully determined the protonation states of substrate and amino acid residues. The carboxyl group of the substrate was treated as being deprotonated (anion), because the optimum pH of L-DEX YL is 9.5. We examined the protonation states of amino acid residues (Asp10, Arg41, Lys151, and Asp180) around the substrate at pH 9.5 with MOE. As a result, Asp10 and Asp180 were treated as anions, while Arg41 and Lys151 were treated as cations.

2.2. QM model and QM/MM (ONIOM) model setting

A structure of a QM model was isolated from the structure of the whole enzyme. The QM model of the enzyme–substrate complex consisted of a QM region, which included the L-2-CPA molecule, a catalytic water, and the side chains of 12 amino acid residues within 5 Å distance around any substrate atom, thus including Asp10, Leu11, Tyr12, Arg41, Leu45, Phe60, Ser118, Asn119, Lys151, Asn177, Trp179, and Asp180 (155 atoms in total). QM calculations were performed mainly using the PM3 [23–25] method and additionally the density functional (B3LYP) [26,27] method with the Gaussian09 program [28]. The model including side chains of all residues of QM region was structurally optimized, while 12 hydrogen atoms replacing α-carbons in each amino acid were fixed during the simulation.

An ONIOM model of the enzyme–substrate complex consisted of two regions, a QM region and an MM region. The QM region was the same as that of the QM model above. The MM region included the whole of the complex (3504 atoms in total). ONIOM [29,30] calculations were performed using the PM3 [23–25] method for the QM region and the Amber 96 force field [31] for the MM region (PM3:Amber) with the Gaussian09 program. One hundred fifty-five atoms including side chains of all residues of the QM region were structurally optimized, while the other atoms were fixed during the simulation.

2.3. TS search and energy profile

Gaussian09 was used for depicting the potential energy curve of the first step reaction, ester intermediate formation, in the dehalogenation reaction catalyzed by L-DEX YL. To validate the PM3 method, the QM calculations were also performed by using the B3LYP/6-31G* [26,27,32,33] method. The internal reaction coordinate was continually moved from the reactants to products. The distance between nucleophilic oxygen atom (OD1) of the aspartic acid (Asp10) and the carbon atom (C5) of the L-2-CPA was allowed to decrease by the increments of 0.1 Å. The structure was fully optimized with the exception of the driving coordinate and 12 hydrogen atoms replacing α-carbon fixed. The TS structure was optimized from the maximum-point structure of the potential energy curve, and then a reactant structure and a product structure were calculated from the TS structure with the intrinsic reaction coordinate (IRC) method [34,35].

The ONIOM calculations were performed by using the QM/MM (PM3:Amber) method. The ONIOM model was scanned from the reactants to the products in the same reaction coordinate as that in the QM calculation with the exception of the driving coordinate and all atoms of the MM region fixed. The TS structure was optimized, and the enzyme–substrate complex and ester intermediate structures were then determined through the minimum energy pathway from the TS structure.

2.4. Calculation of electric charges of important atoms during the reaction

Furthermore, to examine the enzymatic reaction in more detail, we calculated atomic charges around the active site. In the structures of the QM model at each IRC step, Mulliken charges of all atoms were calculated by single-point energy calculations using the PM3 method. The residues observed to transfer charges were used to evaluate the shifts of their Mulliken charges during the reaction.

2.5. Elucidation of the effects of individual amino acid residues

For elucidation of the roles of amino acid residues in the dehalogenation reaction, 11 partial cluster models, containing L-2-CPA,

Asp10, a nucleophile important for the catalytic reaction of L-DEX YL, and 11 kinds of one additional residue of the QM region, were similarly truncated from the series of whole enzyme structures that were obtained from the potential energy curve calculations. They were subjected to single-point calculations using the ONIOM (PM3:Amber) method. Furthermore, to examine the details of the effect of Arg41 (an important residue for the reaction), other three partial cluster models, containing L-2-CPA, Asp10, Arg41 and three kinds of one additional residue (Leu45, Asn177, and Trp179) around Arg41 were similarly truncated from the QM region, and then single-point calculations were performed using the ONIOM (PM3:Amber) method.

2.6. Comparison of the potential energy curve for eight mutant models

Eight mutant models were also constructed by replacing Arg41 with lysine (K), glutamic acid (E), tryptophan (W), alanine (A), glycine (G), homolysine (homK) that contains one more methylene group in the side chain compared to lysine, norlysine (norK) that contains one less methylene group in the side chain compared to lysine, or a sodium ion (Na^+). These models were named R41K, R41E, R41W, R41A, R41G, R41homK, R41norK, and R41Na^+, respectively.

First, the side chain atoms of Arg41 in the wild-type enzyme were replaced with those of each mutated residue by the GaussView5 program [36]. In the case of Na^+, the sodium ion was placed at the nitrogen atom (NH1) position of Arg41 to investigate whether a simple monocation can be substituted for a functional amino acid residue such as Arg or not; if this is the case, the dehalogenation reaction should be controlled by a positive charge and its distance to the halide ion. Second, for each model, the side chain atoms of their mutated amino acid residues were optimized using the ONIOM (PM3:Amber) method with all other atoms of the enzyme fixed; then the structure was fully optimized using the ONIOM (PM3:Amber) method with the exception of the driving coordinate in the QM region and all atoms of the MM region fixed. Finally, the distance between OD1 and C5 was allowed to decrease by the increments of 0.1 Å using the ONIOM (PM3:Amber) method in the same way as in Section 2.3. These potential energy curves of mutants were compared with that of the wild-type.

2.7. Molecular dynamics (MD) calculations

MD simulations of the complexes of L-DEX YL, its R41K and R41homK mutants with L-2-CPA were performed with the similar method to that in Section 2.1. The structures obtained in Section 2.6 were used as the initial structures of the complexes.

In this study, the Amber ff12SB force field [37] was used to parameterize the above complexes instead of ff99SB force field [38]. The constructed complexes were placed into a periodic box and the layer of water molecules was set to be of 15 Å thickness. The initial sizes of the periodic box for the simulations of the wild type, R41K and R41homK mutants were $78.7 \times 81.3 \times 90.2$ Å^3, $95.9 \times 79.7 \times 73.4$ Å^3, and $95.9 \times 79.7 \times 73.4$ Å^3, respectively. They contained 14,556, 14,211, and 14,211 TIP3P water [39,40] molecules, respectively, and four Na^+ counter ions, which were added to keep the whole system electrically neutral. The prep file of homK in the Amber protocol was constructed according to the tutorial of "Generate residue and topology files for non-standard amino acid residues" in the "ANTECHAMBER & GAFF" homepage: http://ambermd.org/antechamber/pro4.html [14/08/2014 last accessed].

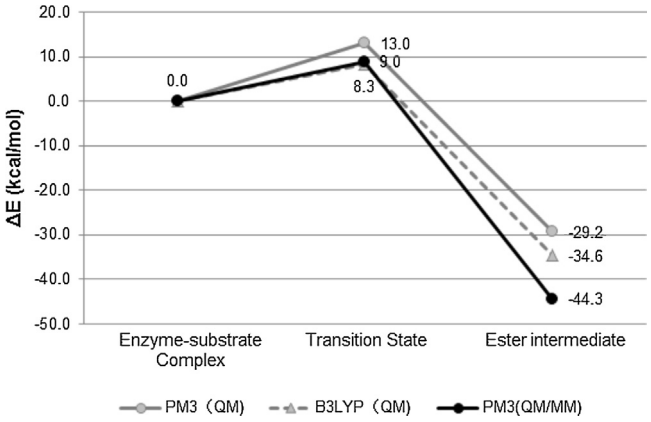

Fig. 2. A comparison of energy profiles among different methods in the ester intermediate formation reaction: QM calculation with PM3 method, closed circles and solid line (gray); QM calculation with B3LYP/6-31G* method, triangles and broken line (gray); QM/MM calculation with PM3:Amber method, closed circles and solid line (black). Potential energy of enzyme–substrate complex was defined to be 0 kcal/mol; relative energies of TS and ester intermediate were calculated as ΔE.

The MD simulations were then performed by the SANDER module of Amber12 [37,41] with the similar method to that in Section 2.1 except for the temperature at 303 K instead of 310 K.

3. Results

3.1. Structures of enzyme–substrate complex, TS, and ester intermediate

The present study determined the TS structure and the energy profile of the dehalogenation reaction of L-2-CPA with L-DEX YL by the QM calculation with the PM3 and B3LYP/6-31G* methods, and also by the ONIOM calculations with the PM3:Amber method, as addressed above.

In the QM calculations using the PM3 method, the TS structure was characterized by a L-2-CPA C5-Asp10 OD1 distance of 2.19 Å and a L-2-CPA C5–Cl6 distance of 2.28 Å. The structure of the enzyme–substrate complex and the ester intermediate were optimized via the IRC method. When the energy of the reactant enzyme–substrate complex is defined to be 0 kcal/mol, those of the TS and ester intermediate structures were 13.0 and −29.2 kcal/mol, respectively. The energy profile is shown in Fig. 2.

Similarly, in the QM calculations with the B3LYP/6-31G* method, the obtained TS structure was characterized by a L-2-CPA C5-Asp10 OD1 distance of 2.35 Å and a L-2-CPA C5–Cl6 distance of 2.31 Å. When the energy of the enzyme–substrate complex is defined to be 0 kcal/mol, those of the TS and ester intermediate structures are 8.3 and −34.6 kcal/mol, respectively (Fig. 2).

By comparing both the TS structures obtained with the PM3 and B3LYP methods, they were found to be almost the same, but the L-2-CPA C5-Asp10 OD1 distance in the B3LYP/6-31G* method was slightly longer than that in the PM3 method (Fig. 3). In addition, there was the difference of orientations of Tyr12 and Phe60. Specifically, in the B3LYP result, Tyr12 turned over toward Arg41 and appeared to mitigate the effect of Arg41 on L-2-CPA, which would thus give a slightly higher activation energy. The energy profiles were different quantitatively, but their features were qualitatively the same. The use of the PM3 method is thus validated for our reactions.

In the ONIOM calculations, the TS structure was characterized by a C5–OD1 distance of 2.39 Å and a C5–Cl6 distance of 2.35 Å (Fig. 4b). The positively charged Arg41 and Lys151 residues roughly constrained the position of the substrate L-2-CPA, and the hydrogen bonds by Tyr12, Ser118, and Lys151 adjusted and fixed

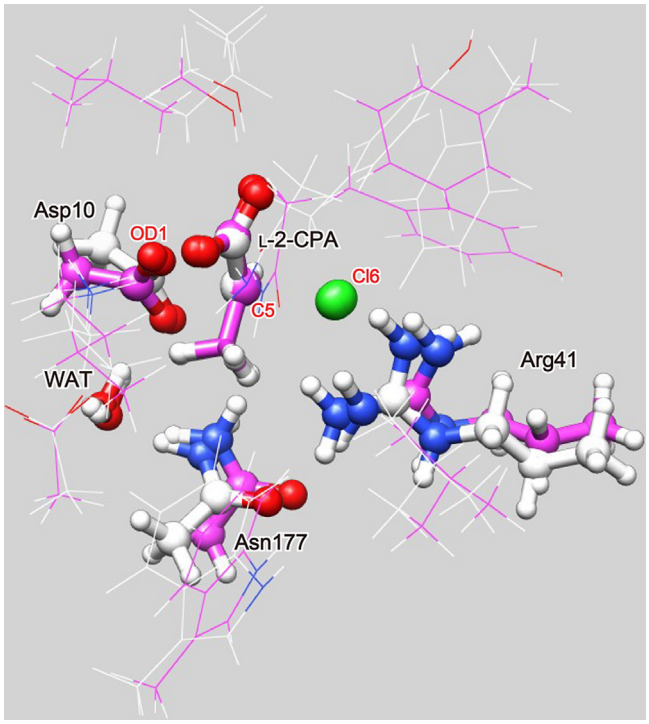

Fig. 3. A comparison of the TS structures obtained by different methods in the QM calculations: with PM3 method, white; with B3LYP/6-31G* method, magenta. Red, blue, gray, white, and green colors mean oxygen, nitrogen, carbon, hydrogen, and chlorine atoms, respectively. There were some differences in orientations of Tyr12 and Phe60, but if they were obtained by QM/MM calculation, there would not be so much differences because amino acid residues around the QM region would suppress their mobile displacements. Illustration was prepared with UCSF Chimera [42]. (For interpretation of the references to color in this figure legend, the reader is referred to the web version of this article.)

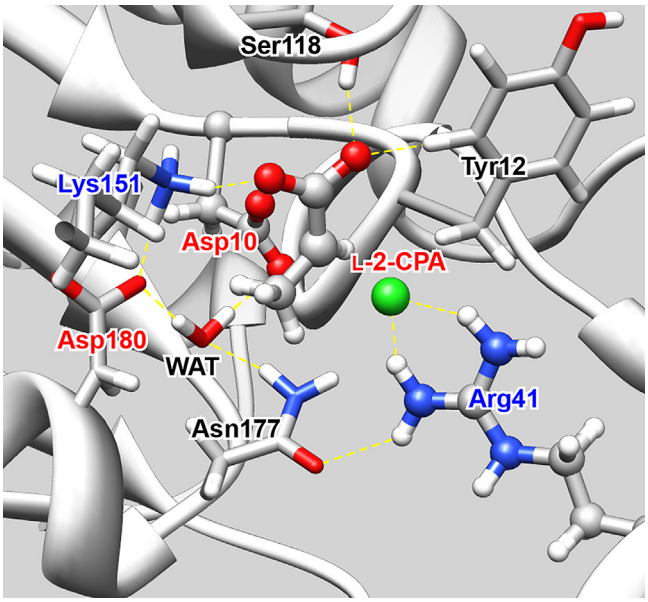

Fig. 5. The hydrogen bond network around L-2-CPA and catalytic water (WAT) at the TS structure of L-DEX YL in the QM/MM calculation with PM3:Amber method. Yellow broken lines mean the hydrogen bonds. Red, blue, gray, white, and green colors mean oxygen, nitrogen, carbon, hydrogen, and chlorine atoms, respectively. Blue and red characters mean positively and negatively charged residues, respectively. Illustration was prepared with UCSF Chimera [42]. (For interpretation of the references to color in this figure legend, the reader is referred to the web version of this article.)

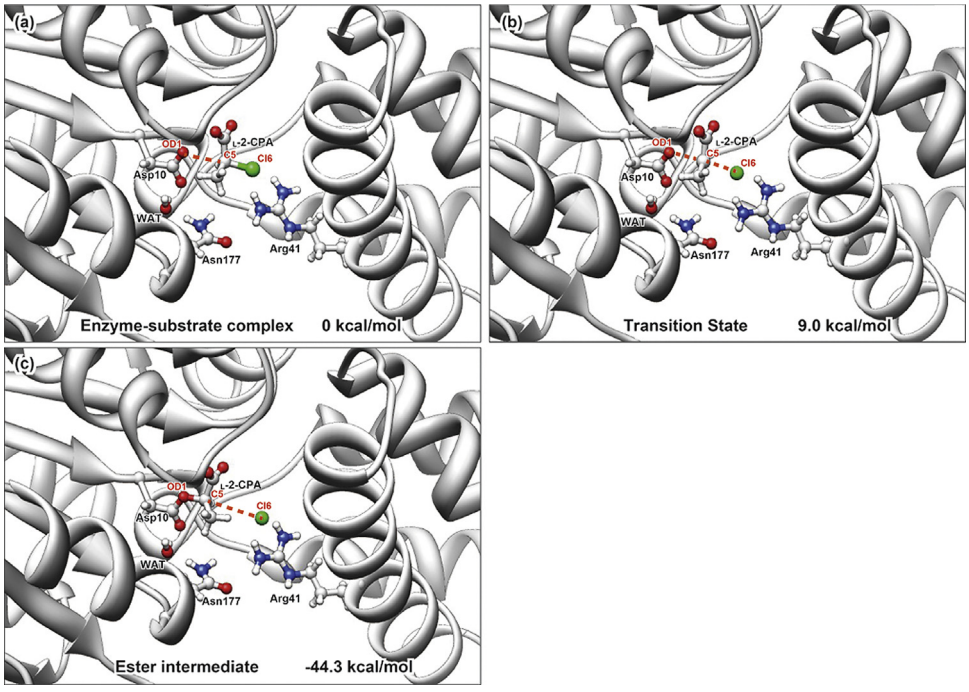

Fig. 4. The active site of the (a) enzyme–substrate complex, (b) transition state, and (c) ester intermediate structures in the QM/MM calculation with ONIOM (PM3:Amber) method. The important parts (L-2-CPA, catalytic water, Asp10, Arg41, and Asn177) were displayed by ball and stick model; illustration was prepared with UCSF Chimera [42]. These structures are characterized by the OD1–C5 distance 2.92 Å, 2.39 Å, and 1.44 Å, the C5–Cl6 distance 1.91 Å, 2.35 Å, and 3.97 Å, and OD1–C5–Cl6 angle 165.24°, 167.44°, and 170.79° for (a) enzyme–substrate complex, (b) transition state, and (c) ester intermediate structures, respectively.

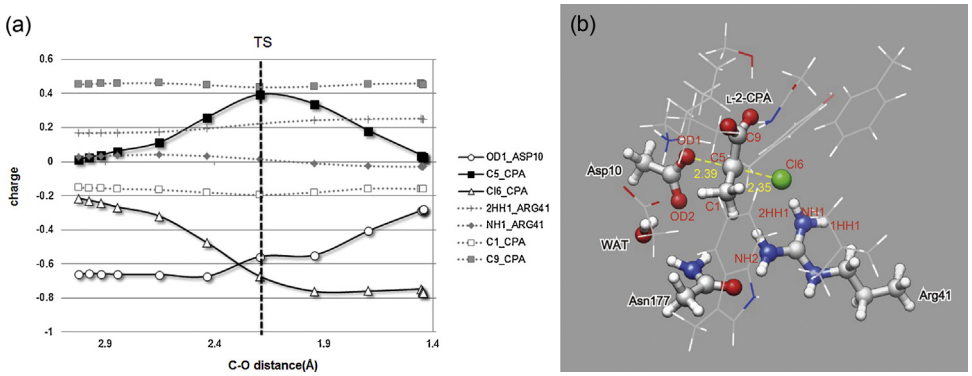

Fig. 6. (a) Charge transfers through the reaction in the QM calculation with PM3 method. The charge of three atoms (OD1, C5, and Cl6) significantly changed: OD1, open circle and solid line (black); C5, closed square and solid line (black); Cl6, open triangle and solid line (black). The charge of the other atoms slightly changed: 2HH1, dotted line with cross (gray); NH1, dotted line with diamond (gray); C1, dotted line with open square (gray); C9, dotted line with closed square (gray). (b) The active site of the TS structure of L-DEX YL, catalytic water, and L-2-CPA in the QM calculation with PM3 method. Two yellow broken lines refer to the most important coordinates in this reaction. Red, blue, gray, white, and green colors mean oxygen, nitrogen, carbon, hydrogen, and chlorine atoms, respectively. Illustration was prepared with UCSF Chimera [42]. (For interpretation of the references to color in this figure legend, the reader is referred to the web version of this article.)

the position and orientation of the L-2-CPA. Catalytic water (WAT), which played an important role in the ester hydrolysis step, was captured by Asp10, Asn177, and Asp180 (Fig. 5). The position of Arg41, which accepts the released chloride ion, was fixed by Asn177. The role of Arg41 was confirmed to be an acceptor of the released chloride ion by electrostatic interaction.

Furthermore, the structures of the enzyme–substrate complex and the ester intermediate were optimized (Fig. 4a and c). When the energy of the enzyme–substrate complex is defined to be 0 kcal/mol, those of the TS and ester intermediate structures are 9.0 and −44.3 kcal/mol, respectively. The energy profiles and the optimized structures are shown in Figs. 2 and 4.

3.2. Charge transfer in the reaction

To examine the reaction in more detail, the electric charges of all the atoms during the reaction were calculated in the QM region model using the PM3 method. Significant charge changes were detected only in Asp10 and CPA; the charge transfers of the main atoms are shown in Fig. 6. When Asp10 OD1 approached L-2-CPA, the charge of the CPA C5 atom changed to a positive value, while that of the chloride ion changed to a more negative value. After the reaction, the C5 charge became almost zero and the charge of the chloride ion changed to an even more negative value, which was accompanied by the decrease in negative charge of OD1 atom of Asp10.

3.3. Effect on the reaction by individual amino acid residue around L-2-CPA

Based on the potential energies of a control group containing L-2-CPA and Asp10, 11 kinds of partial cluster models containing these components and one more amino acid residue were constructed and examined in the potential energy pathway (Fig. 7). The maximum energies in the pathway were found to vary in the models, some more than others. The effect of individual residue was estimated from a comparison of the maximum energies of the 11 kinds of model with that of the control group (Table 1). Here, Arg41 decreased the maximum energy by 42.1 kcal/mol, Lys151 increased it by 23.6 kcal/mol, and Asp180 decreased it by 11.2 kcal/mol, while the other residues showed smaller effects on this step in the reaction model. Thus, these three residues appeared to play important roles in the reaction. In particular, Arg41 residue accepted the released chloride ion as shown in Section 3.1. Moreover, the potential energies of other partial cluster models containing CPA, Asp10, Arg41, and one more other residue near Arg41 were calculated and

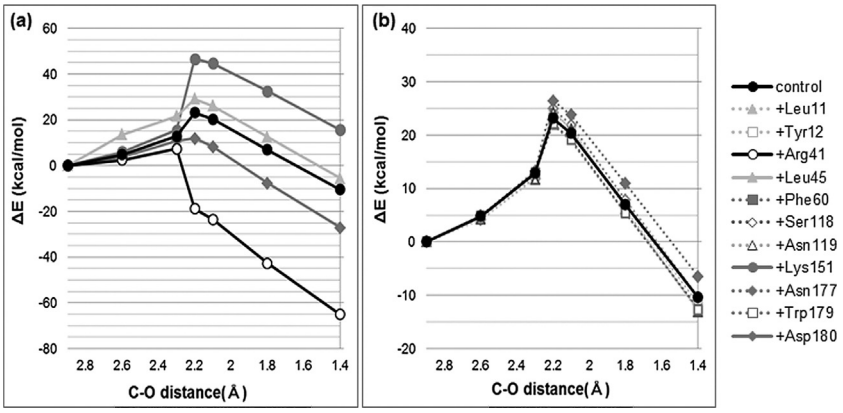

Fig. 7. The reaction pathways of 12 different partial clusters with PM3 method. Control group contained only substrate L-2-CPA and nucleophile Asp10; the other clusters contained L-2-CPA, Asp10, and one additional residue from the active site. (a) Results for control (no additional residue), +Arg41, +Leu45, +Lys151, and +Asp180 are drawn by solid lines with closed circles (black), open circles (black), closed triangles (light gray), closed circles (gray), and closed diamonds (gray), respectively. (b) Results for control, +Leu11, +Tyr12, +Phe60, +Ser118, +Asn119, +Asn177, and +Trp179 are drawn by a solid line with closed circles (black), dotted lines with closed triangles (light gray), open squares (light gray), closed squares (gray), open diamonds (gray), open triangles (gray), closed diamonds (gray), and open squares (gray), respectively. C–O distance means the distance between the OD1 atom of the nucleophile Asp10 and the C5 atom of the attacked L-2-CPA as shown in Fig. 6b. ΔE is defined as the relative difference between the energy of the initial structure and that of each structure in individual cases.

Table 1
The contribution of individual residues to activation energy of the dehalogenation reaction by L-DEX YL calculated with PM3 method.

Residues	$\Delta\Delta E$ (kcal/mol)[a]	Residues	$\Delta\Delta E$ (kcal/mol)[a]
Control	–	Ser118	+1.8
Leu11	+0.3	Asn119	+1.3
Tyr12	+1.1	Lys151	+23.6
Arg41	−42.1	Asn177	+3.3
Leu45	+6.0	Trp179	−1.0
Phe60	−1.2	Asp180	−11.2

[a] The $\Delta\Delta E$ is defined as the relative difference between the energy of L-2-CPA, Asp10 and one additional residue and that of L-2-CPA and Asp10 (control) at the C–O distance 2.2 Å, where the calculated structures are nearly the same as the TS structure.

the effects of the residues were estimated. The potential energy was found to increase by 9.8 kcal/mol due to Asn177, and decrease by 1.6 and 0.5 kcal/mol due to Leu45 and Trp179, respectively. Thus, Asn177 residue appeared to mitigate the stabilization effect of Arg41.

3.4. Effect of mutation at Arg41

The wild-type and eight mutant enzymes at Arg41 were compared in terms of the simulated reaction, produced by displacing the Asp10 OD1 closer to the CPA C5 in the whole enzyme model using the ONIOM (PM3:Amber) method. The comparison of the potential energy curves of the wild-type enzyme and eight mutants at Arg41 is illustrated in Fig. 8. In the R41E, R41W, R41A, and R41G mutants, the potential energies were higher than that of the wild-type at the C5–OD1 distance near the TS structure, and a different reaction occurred; a C1–H bond of methyl group of L-2-CPA was cleaved instead of the C5–Cl6 bond, and a vinyl group was created in the substrate. Moreover, a proton of the methyl group was slightly displaced and the chloride ion was accepted by the proton at the C5–OD1 distance where the reaction coordinate passed over that of the TS structure. Because L-2-CPA became unstable when the distance between Asp10 OD1 and L-2-CPA C5 was too close, these mutants would enter another reaction pathway (Fig. 8b; see also Fig. 11 in Appendix A). In the R41norK mutant, the potential energy was higher than that of the wild-type as well, while the chloride ion was released slightly and made a bond with a proton released from the mutated residue in this case (Fig. 8b; see also Fig. 11). On the other hand, in the R41K, R41homK and R41Na$^+$ mutants, the chloride ion was released and the potential energies were lower than that of the wild-type at the C5–OD1 distance near the TS structure; especially, the maximum energy of R41homK was significantly lower than that of the wild-type enzyme (Fig. 8a).

In Fig. 8, when the peak of the potential energy shifts to the right side of the reaction coordinate, it means that the chloride ion is released late and the transition state becomes unstable. Moreover, mutants might enter another reaction pathway that cleaves the C1–H bond.

4. Discussion

4.1. TS structure and activation energy

In our calculations, the carboxyl group of Asp10 acted as a nucleophile to attack the CPA carbon, resulting in the chloride ion release by an S_N2-type reaction. Here, Arg41 was confirmed to have made a hydrogen bond with the released chloride ion. The structures of TS and the ester intermediate in this study were similar to the reported structures of haloalkane dehalogenase [15,16] and fluoroacetate dehalogenase [17,43]. In these enzymes, TS structures possess an attacking aspartic acid residue located on one side of the substrate, halide ion acceptors such as arginine, tryptophan, histidine and tyrosine located on the opposite side of the aspartic acid, and some amino acid residues fixing the position of the substrate. The haloalkane dehalogenase has two halide ion acceptors, and the

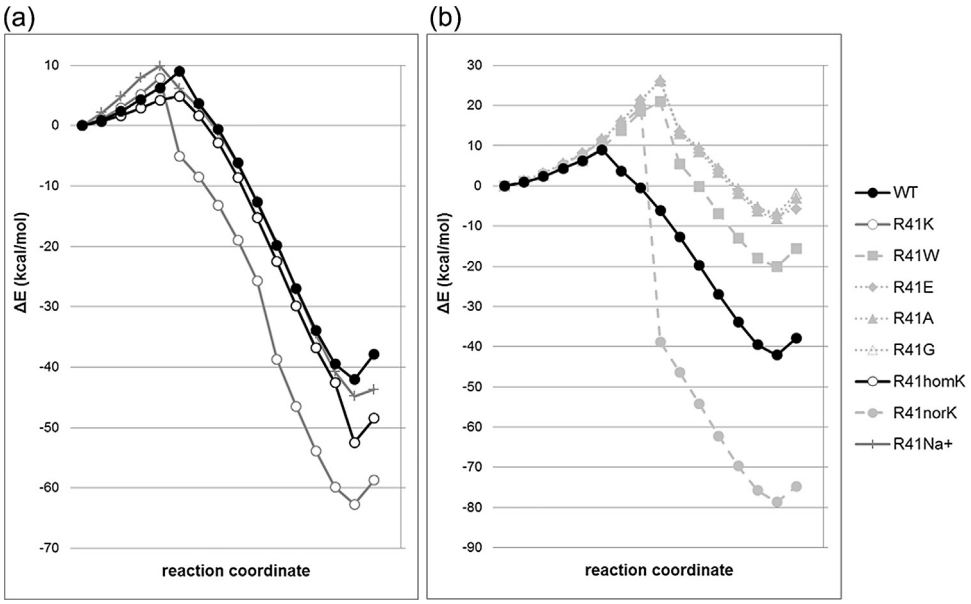

Fig. 8. Comparison of the potential energy curves of the wild-type enzyme and eight mutants at Arg41. We referred to the mutant enzymes that replaced Arg41 by lysine, tryptophan, glutamic acid, alanine, glycine, homolysine (one more methylene group in the side chain compared to lysine), norlysine (one less methylene group in the side chain compared to lysine), and a sodium ion as R41K, R41W, R41E, R41A, R41G, R41homK, R41norK, and R41Na$^+$, respectively. Line and symbol styles mean as follows: (a) the reaction preferred cases drawn by solid lines: wild-type (WT), closed circles and solid line (black); R41K, open circles and solid line (gray); R41homK, open circles and solid line (black); R41Na$^+$, crosses and solid line (gray). (b) The reaction unpreferred cases drawn by broken lines and dotted lines: R41W, closed squares and broken line (gray); R41norK, closed circles and broken line (gray); R41E, closed diamonds and dotted line (gray); R41A, closed triangles and dotted line (gray); R41G, open triangles and dotted line (gray). The reaction was simulated by moving Asp10 oxygen atom OD1 closer to L-2-CPA carbon atom C5 as shown in Fig. 6b. Reaction coordinate is proportional to the distance between the OD1 atom of the nucleophile Asp10 and the C5 atom of the attacked L-2-CPA, and the reaction proceeds from left to right in these figures. ΔE is defined as the relative difference between the energy of the initial structure and that of each structure in individual cases.

fluoroacetate dehalogenase has three halide ion acceptors. From these observations, the enzyme that has more halide ion acceptors would be capable of cleaving a stronger carbon–halogen bond.

The activation energy for the dehalogenation reaction between L-2-CPA and L-DEX YL was calculated to be 9.0 kcal/mol with the ONIOM method (Fig. 2). Our activation barrier was higher than that of the fluoroacetate dehalogenase although the C–F bond is stronger than the C–Cl bond. The activation energy of the latter was calculated to be 2.7 kcal/mol at high pH (9.5) and 5.8 kcal/mol at low pH (7.0) by the B3LYP/6-311++G** method [44,45], while the B3LYP method may underestimate the activation barrier [43]. Our QM model calculations also suggested that the B3LYP method gave a lower activation energy than the PM3 method as shown in Fig. 2. L-DEX has less halide ion acceptors, and we used the PM3 method in the ONIOM calculations. Thus we suppose that our activation barrier, which may seem somewhat high, would be reasonable.

4.2. The roles of amino acid residues in the catalytic reaction

The hydrogen bond interaction between the L-2-CPA and Arg41 appeared to be the most important factor in lowering the activation barrier for the C–Cl bond cleavage as shown in Fig. 7. This computational result was consistent with the experimental result where an R41K mutant lost enzymatic activity in site-directed mutagenesis [6] and indicated that arginine would accept the chloride ion, as suggested by crystal structural analysis [9].

In addition, Asn177 appeared to play an important role, mitigating the effect of Arg41, and Arg41 and Asn177 residues control the activation energy in the ester intermediate formation step, whose detailed mechanism remains to be elucidated. The roles of Lys151 and Asp180 in this step were also investigated. Fig. 5 shows the hydrogen bond network around L-2-CPA and catalytic water. Lys151, Asn177 and Asp180 appeared to control the rotation of L-2-CPA and Asp10, which attacks L-2-CPA, and the position of the water molecule, which attacks the ester intermediate, by forming a hydrogen bond network. These results were consistent with earlier simulations of the molecular dynamics of this enzyme [14].

The enzyme L-DEX YL does not have the histidine that is one of the catalytic triad seen in serine protease and haloalkane dehalogenase [46]. In the present study, an alternative amino acid residue for histidine was not revealed, but this feature will be investigated in a future study of the ester hydrolysis step, which is under way in our research group.

4.3. The role of mutated amino acid residues at Arg41 for activation energy

The potential energy curves of the wild-type and eight mutant enzymes at Arg41 were compared (Fig. 8). The differences among the eight mutants were mainly detected in terms of the atomic distance from the chloride ion to the nitrogen atom in the side chain at the replaced residue (Table 2). As the tryptophan of R41W, the glutaminic acid of R41E, the alanine of R41A, and the glycine of R41G did not have a positive charge at the replaced residue and could not accept the chloride ion, the reaction could not occur. With respect to tryptophan, some factors except for electric charge may be related to the activation energy because tryptophan accepts the halide ion released by the dehalogenation reaction in the haloalkane dehalogenase [15,16]. The activation energy of R41norK was higher than that of the wild-type because norK is shorter than lysine by one methylene group. The sodium ion was set at the same distance from the chloride ion of L-2-CPA as the nitrogen atom (NH1) of the wild-type Arg41, and the activation energy of R41Na$^+$ was similar to that of the wild-type. Moreover, the side chains of lysine of

Table 2
Relation between activity and distance of Y-Cl.

Variant	E_{max}[a] (kcal/mol)	Specific activity (U/mg)[b]	Distance of Y–Cl in initial structure (Å)[c]
Wild-type	9.02	100	3.22
R41K	7.89	0.19	3.07
R41W	20.96	0	5.40
R41E	25.98	0.05	–[e]
R41A	26.19	–[d]	–[e]
R41G	26.20	–[d]	–[e]
R41homK	4.87	–[d]	2.81
R41norK	19.39	–[d]	4.69
R41Na$^+$	9.91	–[d]	2.89[f]

[a] The maximum value of ΔE in the individual potential curves shown in Fig. 8.
[b] The activities refer to the experimental values obtained by Kurihara et al. [6].
[c] The distance between the nitrogen atom in the side chain or sodium ion (Y) at the replaced residue and the chloride ion Cl6 released from L-2-CPA.
[d] Not determined.
[e] Not studied because there is no nitrogen atom in the side chain.
[f] The Na$^+$ ion was placed at the nitrogen atom (NH1) position of Arg41 that has the closest hydrogen atom (2HH1) to Cl6.

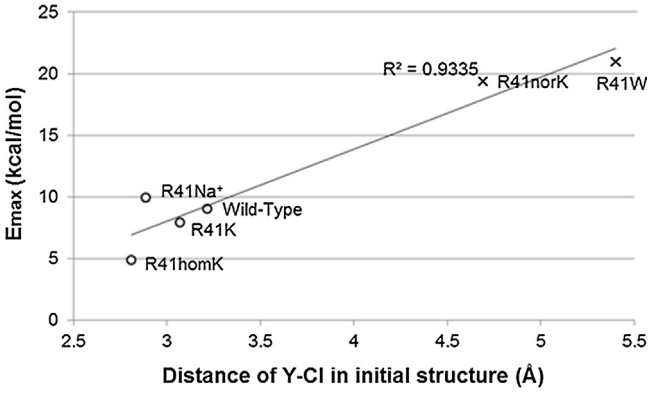

Fig. 9. Correlation between the distance of Y–Cl and E_{max} in Table 2. Open circle and cross mean the reaction preferred and unpreferred cases as shown in Fig. 8, respectively. The distance means the atomic distance between the nitrogen atom in the side chain or sodium ion (Y) at the replaced residue and the negatively charged chloride ion Cl6 released from L-2-CPA.

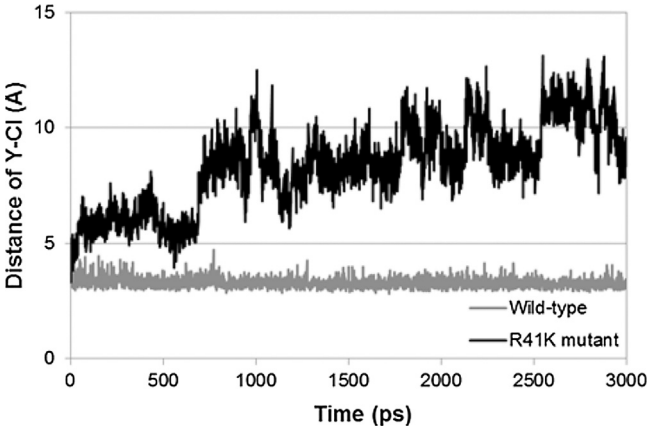

Fig. 10. The result of MD simulation of the R41K mutant and wild-type. Black and gray lines refer to the results of the R41K mutant and the wild-type, respectively. Since the distance increased beyond 5 Å during 3 ns simulation, the lysine could not accept the chloride ion. Y means the nitrogen atom in the side chain.

R41K and homK are longer than that of arginine, and the calculated activation energies of R41homK and R41K were lower than that of the wild-type. Thus, the distance from the chloride ion to the nitrogen atom in the side chain seems to dictate the activation energy (Fig. 9).

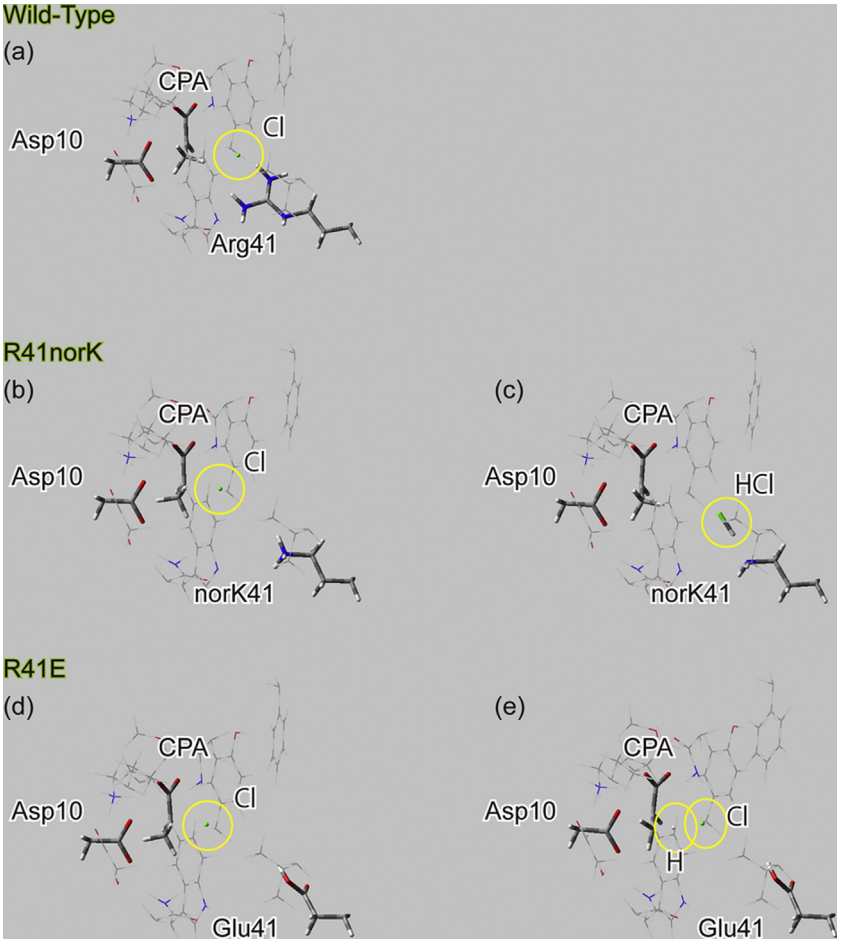

Fig. 11. (a) The wild-type structure at the next coordinate point of the peak position in the potential energy curve releasing the chloride ion from the L-2-CPA, which is accepted by Arg41. (b) The R41norK structure at the same reaction coordinate as the wild-type enzyme which holds the chloride ion still. (c) The R41norK structure at the next coordinate point of its energy peak position releasing the chloride ion which makes a bond to a proton released from the mutated residue. Thus the associated potential energy decreased dramatically in this process. (d) The R41E structure at the same reaction coordinate as the wild-type enzyme which holds the chloride ion still. (e) The R41E structure at the next coordinate point of its energy peak position with a vinyl group produced in the substrate, where a proton of the methyl group is slightly released and accepts the chloride ion. Red, blue, gray, white and green colors mean oxygen, nitrogen, carbon, hydrogen and chlorine atoms, respectively. Illustration was prepared with GaussView [36]. (For interpretation of the references to color in this figure legend, the reader is referred to the web version of this article.)

However, we may have one conflicting element of data in the experiment as seen in Table 2. The R41W, R41E and R41K mutants have been studied in site-directed mutagenesis [6]; the specific activities of the mutants toward L-2-CPA were lower than 0.2% of that of the wild-type enzyme. Though the R41K mutant lacked the specific activity as seen in the experiment in 1995 [6], the R41K mutant did have a lower activation energy than that of the wild-type in our simulation. We then ran an additional simulation to examine the cause. MD simulations starting from their initial structures showed a notable difference between the wild-type and R41K mutant (Fig. 10). In the wild-type, Arg41 was positioned near the CPA to accept the released chloride ion. On the other hand, Lys41 was not positioned near the CPA in the R41K mutant. This result suggested that the R41K mutant could not undergo the reaction relevantly. Thus the discrepancy between a result of our QM/MM simulation of the R41K mutant and the experiment may be accounted for (see Fig. 10). In addition, the catalytic water was observed to escape from the active site in the case of R41K mutant, which should be unfavorable for the following ester hydrolysis reaction. It is noted here that the experimental specific activities [6] should correspond to the entire reaction rates described in Fig. 1. Even if the reaction was delayed, R41K could form the ester intermediate, as has been shown in mass spectrometric analyses [9]. The agreement of these two experimental studies with the present simulations might mean that, while most R41K complexes do not overcome the activation barrier, low-abundance complexes fortuitously may do so. On the other hand, in the case of R41homK mutant, we observed that the calculated energy barrier was significantly lower than that of the wild type. Although the MD simulation showed that the homK was not positioned near the CPA in the R41homK mutant, the catalytic water was retained in the reaction region, thus providing a favorable condition for the following ester hydrolysis reaction. Taken together, we may expect that the R41homK mutant (data not shown) could be active as well as the wild-type enzyme.

5. Conclusions

The TS structure and the energy profile of the ester intermediate formation step of L-DEX YL with L-2-CPA were elucidated and the reaction mechanism in this step was analyzed along with the roles of residues in the active site on the basis of ONIOM calculations. The activation energy of the reaction was demonstrated to be controlled mainly by Arg41, and Asn177 was found to mitigate the stabilization effect of Arg41 during the ester intermediate formation. Furthermore, eight mutant enzymes at Arg41 were compared by mutagenesis simulations and the results suggested that the R41homK mutant enzyme, which possesses a longer

side chain than lysine or arginine, could dehalogenate L-2-CPA as efficiently as the wild-type enzyme. The distance from the chloride ion to the position of the positive charge of the acceptor seems to dictate the activation energy.

Acknowledgements

We appreciate the fruitful discussions with members of Tanaka Laboratory and Ebina Laboratory at Kobe University. We used the computer resources at the Information Science and Technology Center at Kobe University, those of the Cyber Media Center at Osaka University, Information Technology Center at Nagoya University, and those of the Research Center for Computational Science, Okazaki Research Facilities, National Institutes of Natural Sciences.

Appendix A. Behaviors of released chloride ion

In Fig. 11 we depict typical behaviors of released chloride ion in the wild-type and mutant enzymes, where the QM region structures in the ONIOM calculations in Section 2.6 are shown. Fig. 11a illustrates the wild-type structure which represents the reaction structure similar to the R41K, R41homK and R41Na$^+$ mutants. Fig. 11b and c shows the structures of R41norK mutant whose chloride ion were released slightly, but catalytic reaction would not occur because of the high activation barrier. Fig. 11d and e demonstrates the structures of R41E mutant whose catalytic reaction did not occur analogously to the R41W, R41A and R41G mutants.

References

[1] G.W. Gribble, Chemosphere 52 (2003) 289–297.
[2] T. Kurihara, Biosci. Biotechnol. Biochem. 75 (2011) 189–198.
[3] D. O'Hagan, J.W. Schmidberger, Nat. Prod. Rep. 27 (2010) 900–918.
[4] J.Q. Liu, T. Kurihara, A.K.M.Q. Hasan, V. Nardi-Dei, H. Koshikawa, N. Esaki, K. Soda, Appl. Environ. Microbiol. 60 (1994) 2389–2393.
[5] A.K.K.Q. Hasan, H. Takada, H. Koshikawa, J.Q. Liu, T. Kurihara, N. Esaki, K. Soda, Biosci. Biotechnol. Biochem. 58 (1994) 1599–1602.
[6] T. Kurihara, J.Q. Liu, V. Nardi-Dei, H. Koshikawa, N. Esaki, K. Soda, J. Biochem. 117 (1995) 1317–1322.
[7] T. Hisano, Y. Hata, T. Fujii, J.Q. Liu, T. Kurihara, N. Esaki, K. Soda, J. Biol. Chem. 271 (1996) 20322–20330.
[8] Y.F. Li, Y. Hata, T. Fujii, T. Hisano, M. Nishihara, T. Kurihara, N. Esaki, J. Biol. Chem. 273 (1998) 15035–15044.
[9] Y.F. Li, T. Fujii, T. Kurihara, N. Esaki, J. Biochem. 124 (1998) 20–22.
[10] J.Q. Liu, T. Kurihara, M. Miyagi, S. Tsunakawa, M. Nishihara, N. Esaki, K. Soda, J. Biol. Chem. 272 (1997) 3363–3368.
[11] S. Ichiyama, T. Kurihara, Y.F. Li, Y. Kogure, S. Tsunasawa, N. Esaki, J. Biol. Chem. 275 (2000) 40804–40809.
[12] Y.F. Li, T. Kurihara, S. Ichiyama, M. Miyagi, S. Tsunasawa, N. Esaki, J. Mol. Catal. B: Enzym. 23 (2003) 337–345.
[13] J.Q. Liu, T. Kurihara, M. Miyagi, N. Esaki, K. Soda, J. Biol. Chem. 270 (1995) 18309–18312.
[14] T. Nakamura, A. Yamaguchi, H. Kondo, H. Watanabe, T. Kurihara, N. Esaki, S. Hirono, S. Tanaka, J. Comput. Chem. 30 (2009) 2625–2634.
[15] J. Damborský, M. Kutý, M. Němec, J. Koča, J. Chem. Inf. Comput. Sci. 37 (1997) 562–568.
[16] M. Kutý, J. Damborský, M. Prokop, J. Koča, J. Chem. Inf. Comput. Sci. 38 (1998) 736–741.
[17] T. Kamachi, T. Nakayama, O. Shitamachi, K. Jitsumori, T. Kurihara, N. Esaki, K. Yoshizawa, Chem. Eur. J. 15 (2009) 7394–7403.
[18] J.W. Schmidberger, J.A. Wilce, J.S.H. Tsang, M.C.J. Wilce, J. Mol. Biol. 368 (2007) 706–717.
[19] MOE, Ver. 2006.08, Chemical Computing Group, Montreal, Canada.
[20] H. Edelsbrunner, M. Facello, R. Fu, J. Liang, Proceeding of the 28th Hawaii International Conference on System Science, Hawaii, 1995, pp. 256–264.
[21] J. Goto, R. Kataoka, H. Muta, N. Hirayama, J. Chem. Inf. Model. 48 (2008) 583–590.
[22] D.A. Case, T.A. Darden, T.E. Cheatham III, C.L. Simmerling, J. Wang, R.E. Duke, R. Luo, K.M. Merz, B. Wang, D.A. Pearlman, M. Crowley, S. Brozell, V. Tsui, H. Gohlke, J. Mongan, V. Hornak, G. Cui, P. Beroza, C. Schafmeister, J.W. Caldwell, W.S. Ross, P.A. Kollman, AMBER 8, University of California, San Francisco, 2004.
[23] J.J.P. Stewart, J. Comput. Chem. 10 (1989) 209–220.
[24] J.J.P. Stewart, J. Comput. Chem. 10 (1989) 221–264.
[25] E. Anders, R. Koch, P. Freunscht, J. Comput. Chem. 14 (1993) 1301–1312.
[26] A.D. Becke, J. Chem. Phys. 98 (1993) 5648–5652.
[27] P.J. Stephens, F.J. Devlin, C.F. Chabalowski, M.J. Frisch, J. Phys. Chem. 98 (1994) 11623–11627.
[28] M.J. Frisch, G.W. Trucks, H.B. Schlegel, G.E. Scuseria, M.A. Robb, J.R. Cheeseman, G. Scalmani, V. Barone, B. Mennucci, G.A. Petersson, H. Nakatsuji, M. Caricato, X. Li, H.P. Hratchian, A.F. Izmaylov, J. Bloino, G. Zheng, J.L. Sonnenberg, M. Hada, M. Ehara, K. Toyota, R. Fukuda, J. Hasegawa, M. Ishida, T. Nakajima, Y. Honda, O. Kitao, H. Nakai, T. Vreven, J.A. Montgomery Jr., J.E. Peralta, F. Ogliaro, M. Bearpark, J.J. Heyd, E. Brothers, K.N. Kudin, V.N. Staroverov, R. Kobayashi, J. Normand, K. Raghavachari, A. Rendell, J.C. Burant, S.S. Iyengar, J. Tomasi, M. Cossi, N. Rega, J.M. Millam, M. Klene, J.E. Knox, J.B. Cross, V. Bakken, C. Adamo, J. Jaramillo, R. Gomperts, R.E. Stratmann, O. Yazyev, A.J. Austin, R. Cammi, C. Pomelli, J.W. Ochterski, R.L. Martin, K. Morokuma, V.G. Zakrzewski, G.A. Voth, P. Salvador, J.J. Dannenberg, S. Dapprich, A.D. Daniels, Ö. Farkas, J.B. Foresman, J.V. Ortiz, J. Cioslowski, D.J. Fox, Gaussian 09, Revision A.1, Gaussian, Inc., Wallingford, CT, 2009.
[29] S. Dapprich, I. Komáromi, K.S. Byun, K. Morokuma, M.J. Frisch, J. Mol. Struct. 462 (1999) 1–21.
[30] T. Vreven, K. Morokuma, Ö. Farkas, H.B. Schlegel, M.J. Frisch, J. Comput. Chem. 24 (2003) 760–769.
[31] W.D. Cornell, P. Cieplak, C.I. Bayly, I.R. Gould, K.M. Merz Jr., D.M. Ferguson, D.C. Spellmeyer, T. Fox, J.W. Caldwell, P.A. Kollman, J. Am. Chem. Soc. 117 (1995) 5179–5197.
[32] W.J. Hehre, R. Ditchfield, J.A. Pople, J. Chem. Phys. 56 (1972) 2257–2261.
[33] P.C. Hariharan, J.A. Pople, Theor. Chim. Acta 28 (1973) 213–222.
[34] K. Fukui, J. Phys. Chem. 74 (1970) 4161–4163.
[35] K. Fukui, Acc. Chem. Res. 14 (1981) 363–368.
[36] R. Dennington, T. Keith, J. Millam, GaussView, Version 5, Semichem Inc., Shawnee Mission, KS, 2009.
[37] D.A. Case, T.A. Darden, T.E. Cheatham III, C.L. Simmerling, J. Wang, R.E. Duke, R. Luo, R.C. Walker, W. Zhang, K.M. Merz, B. Roberts, S. Hayik, A. Roitberg, G. Seabra, J. Swails, A.W. Goetz, I. Kolossváry, K.F. Wong, F. Paesani, J. Vanicek, R.M. Wolf, J. Liu, X. Wu, S.R. Brozell, T. Steinbrecher, H. Gohlke, Q. Cai, X. Ye, J. Wang, M.J. Hsieh, G. Cui, D.R. Roe, D.H. Mathews, M.G. Seetin, R. Salomon-Ferrer, C. Sagui, V. Babin, T. Luchko, S. Gusarov, A. Kovalenko, P.A. Kollman, Amber12, University of California, San Francisco, 2012.
[38] V. Hornak, R. Abel, A. Okur, B. Strockbine, A. Roitberg, C. Simmerling, Proteins 65 (2006) 712–725.
[39] W.L. Jorgensen, J. Chandrasekhar, J.D. Madura, R.W. Impey, M.L.J. Klein, J. Chem. Phys. 79 (1983) 926–935.
[40] E. Neria, S. Fischer, M. Karplus, J. Chem. Phys. 105 (1996) 1902–1921.
[41] R. Salomon-Ferrer, D.A. Case, R.C. Walker, WIREs Comput. Mol. Sci. 3 (2013) 198–210.
[42] E.F. Pettersen, T.D. Goddard, C.C. Huang, G.S. Couch, D.M. Greenblatt, E.C. Meng, T.E. Ferrin, J. Comput. Chem. 13 (2004) 1605–1612.
[43] T. Nakayama, T. Kamachi, K. Jitsumori, R. Omi, K. Hirotsu, N. Esaki, T. Kurihara, K. Yoshizawa, Chem. Eur. J. 18 (2012) 8392–8402.
[44] R. Krishnan, J.S. Binkley, R. Seegar, J.A. Pople, J. Chem. Phys. 72 (1980) 650–654.
[45] T. Clark, J. Chandrasekhar, G.W. Spitznagel, P.v.R. Schleyer, J. Comput. Chem. 4 (1983) 294–301.
[46] J.Q. Liu, T. Kurihara, N. Esaki, K. Soda, J. Biochem. 116 (1994) 248–249.